AAEC/E 130

AUSTRALIAN ATOMIC ENERGY COMMISSION

RESEARCH ESTABLISHMENT

LUCAS HEIGHTS

EXAMINATION OF BeO IRRADIATED AT ELEVATED TEMPERATURES IN THE ENGINEERING TEST REACTOR

by

B. S. HICKMAN

J. CHUTE

Issued Sydney, September 1964

AUSTRALIAN ATOMIC ENERGY COMMISSION

RESEARCH ESTABLISHMENT

LUCAS HEIGHTS

EXAMINATION OF BeO IRRADIATED AT ELEVATED TEMPERATURES IN THE ENGINEERING TEST REACTOR

by

B. S. HICKMAN

J. CHUTE

ABSTRACT

A description is given of an examination of BeO samples irradiated by the General Electric Co. in the Engineering Test Reactor, Idaho Falls, to doses up to 1.2×10^{21} (> 1 MeV) and temperatures in the range 470 – 1200 °C, at dose rates of 1 to 3×10^{14} nv.

The results of X–ray measurements and optical and electron microscopy are presented and discussed. Comparisons are made with previously reported results on similar material irradiated in the reactor HIFAR at lower dose rates.

CONTENTS

1. INTRODUCTION

In this report a description is given of an examination at Lucas Heights of some irradiated beryllium oxide supplied by the Nuclear Materials and Propulsion Operation, General Electric Co., U.S.A. The samples were irradiated in the Engineering Test Reactor at Idaho Falls at 470 – 1200 °C to doses ranging up to 1.2×10^{21} nvt > 1 MeV.

The purpose of this work was threefold:

(i) To make a direct comparison of the experimental techniques of the two laboratories by comparing results from pieces of the same samples. This would then enable a more direct comparison of our data with the large amount of data collected by N.M.P.O.

(ii) To enable the Research Establishment to obtain some direct information on behaviour in the temperature range 800 – 1200 °C in advance of the availability of its own samples; most of the samples were irradiated at higher temperatures than have so far been achieved with samples in HIFAR.

(iii) To obtain information on the effect of dose rate on the damage. Some samples were irradiated in the same temperature range, and to similar doses, as the Lucas Heights samples, but at ten times the dose rate.

2. EXPERIMENTAL

2.1 Material

The two types of material were extruded and sintered Brush UOX containing 0.5 wt. per cent. MgO, and extruded and sintered Brush AOX. The samples were supplied as broken bend test pieces.

Fabrication methods, properties of the unirradiated material, and irradiation details are given by General Electric (1963). The samples are listed in Table 1 together with the irradiation flux, dose, and temperature, and data on dimensional changes as supplied by N.M.P.O. The samples covered a range of grain sizes (from 5μ to 80μ) and densities (2.75 or 2.90 g/cm^3).

2.2 Measuring Techniques

Lattice parameter measurements were made using an 11.43 cm powder camera. Specimens were prepared by grinding the samples and the parameters were computed from the measured reflections using a least squares analysis (Walker 1963). The sharp components of h k ℓ reflections for $\ell \neq 0$ were used to determine the c parameter as described by Walker, Mayer, and Hickman (1964).

The integral breadths of the 300 CuKα reflections were measured on solid samples using a diffractometer scanning at one tenth of a degree per minute and corrections for instrumental broadening were made by subtracting the integral breadth of unirradiated material. For optical microscopy examination samples were ground and then hand polished on a 0–1μ diamond lap. For electron microscope examinations replicas were taken from fracture surfaces. Thin flakes were often stripped off by the replica and were examined by direct transmission; to avoid further damage to the specimens by the electron beam, the examination was carried out using an accelerating voltage of 60 kV.

3. RESULTS AND DISCUSSION

3.1 X-ray Diffraction Studies

The results of the lattice parameter measurements are summarised in Table 2 which also shows the volume changes computed from the lattice parameters and the macroscopic volume changes as measured by N.M.P.O. Examination of the films showed that the relative intensity of the sharp component of the h k ℓ reflections for $\ell \neq 0$ showed similar trends with temperature to those observed by Walker et al. (1964), that is, the intensity of the sharp component decreased with increasing temperature at a given dose.

In Figure 1 the $\underset{\sim}{c}$ parameter changes are compared with those measured on A.A.E.C. material irradiated in HIFAR (Walker et al. 1964). All results are normalised to 10^{21} nvt > 1 MeV assuming a linear relation between $\underset{\sim}{c}$ parameter and dose. In general the present results are compatible with those of Walker et al. showing with increasing irradiation temperatures a decrease in $\underset{\sim}{c}$ parameter change to very low values at around 1000 °C. The scatter is rather large but within the limits which could be explained by errors in temperature and dose. However, there are two exceptions:

(i) Samples irradiated at 1200 °C all showed larger parameter changes than samples irradiated at 1000 °C and in fact showed similar changes to samples irradiated at 700 – 800 °C, (this effect is discussed in Section 3.4).

(ii) Sample 226–31 irradiated at 475 °C gave an anomalously low figure. The dose would have to be in error by a factor of 2 or the temperature by 250 °C to bring this result into line with the others. No explanation can be offered for this effect.

The $\underset{\sim}{a}$ parameter change was negligible in all samples except 226–31.

If these anomalies are neglected, the results suggest that dose rate had no major effect on the total damage, at least within the range $2–3 \times 10^{13}$ nv used in our own work and $1–3 \times 10^{14}$ used by N.M.P.O. Small effects may have been obscured by the wide scatter in results.

The integral line breadths of the 300 CuK_α reflection are also given in Table 2. Hickman et al. (1962) and Walker et al. (1964) showed that below 700 °C this line broadening was due to intergranular strain arising from anisotropic growth and the extent of the broadening in the absence of microcracking can be directly related to $\Delta c/c - \Delta a/a$. When the $\underset{\sim}{c}$ parameter change, plotted against 300 line broadening in the present samples (Figure 2), is compared with the results of Walker et al. (1964) it is clear that in samples irradiated above 800 °C there is much more line broadening than would be expected from the $\underset{\sim}{c}$ parameter change. (Note: sample 226–31 is again anomalous). This could be due to:

(i) Line broadening due to defect clustering. This has not been observed in {h, k, O } reflections below 800 °C but may occur above this temperature. This should still be observable in powder photographs.

(ii) Anisotropic growth which is not reflected in corresponding lattice parameter changes. This will not be observable in powder photographs of crushed specimens.

Examination of powder photographs of these samples shows some broadening still present but not nearly sufficient to account for the broadening in the solid specimens. It appears likely therefore that there was some contribution to the line broadening, by anisotropic dimensional changes, which did not produce a lattice parameter change. This could arise from formation of pure interstitial dislocation loops perpendicular to the $\underset{\sim}{c}$ axis; if the vacancies from which these interstitials originated are still present, there will also be a macroscopic volume change which is not reflected in the lattice parameters.

In the samples irradiated at around 1000 °C the macroscopic volume change exceeded the X–ray volume change by up to 0.5 per cent; this could be due to:

(i) Microcracking.

(ii) Helium bubble formation.

(iii) Pure loop formation as discussed above.

The observed microcracking in these samples is thought to be insufficient to explain the discrepancy. Unfortunately (see Section 3.3) it is not possible to measure the volume change due to helium and hence one cannot distinguish between helium bubble formation and pure loop formation. The arguments outlined above, however, suggest that the loop formation could be significant.

3.2 Optical Microscopy

A limited number of samples were examined by optical microscopy and the results are summarised in Table 4. The measured grain sizes were of the same order although smaller than the nominal grain sizes quoted by General Electric. The observation of microcracking in samples 130-5, 130-31, and 153-23, all of which were irradiated at 1000 - 1100 °C and showed very small lattice parameter changes, is of interest. (130-31 showed no measurable $\underset{\sim}{c}$ parameter change at all). Even allowing for the coarse grain size of these materials it is considered that the observed $\underset{\sim}{c}$ change was insufficient to cause microcracking. This is therefore further evidence for the presence of anisotropic crystal growth which did not produce a corresponding $\underset{\sim}{c}$ parameter change. Samples 153 - 23 and 130 - 5 (Figure 3) showed extensive void formation at grain boundaries which is attributed to helium bubble formation. Often these voids were linked by cracks. This could have been a contributing factor to the observed microcracking but is not considered primarily responsible as cracks could often be observed where no void formation was visible and transgranular cracking also occurred.

3.3 Electron Microscopy

The results of electron microscopy observations are summarised in Table 3. One feature of many samples of this material was that flakes of basal-plane orientation were often obtained as well as prism-plane flakes. Previously in examination of our own material it had only been possible to obtain prism-plane flakes. The following significant observations of defect clusters and loops were made on these flakes:

(i) Samples irradiated at 470 °C (226 - 31), 750 °C (202 - 8), 840 °C (117 - 6), 895 °C (202 - 11), and at 1000 - 1100 °C (169 - 8, 153 - 23), all showed defect clusters and loops, most of which were parallel to the basal plane. The loop size increased with increasing temperature (see Figures 4 and 5) and at 1000 - 1100 °C, loops were mostly in the 500 - 2000 Å range. The loop size and density in these samples were generally quite compatible with our own observations (Chute and Walker 1964). The loops examined in the basal plane flakes appeared quite free of contrast effects in the centre of the loop (Figure 5d).

(ii) All other samples showed somewhat anomalous behaviour as follows:

(a) Samples irradiated at 1200 °C (315 - 20, 202 - 30, 305 - 27, and 227 - 30), Figure 6, all showed characteristic loop defect formation parallel to the basal planes but their size range (200 - 600 Å) was considerably lower than for samples irradiated at 1000 - 1100 °C, that is, the trend of increasing loop size with increasing temperature had been reversed. In one flake of sample 202 - 30 there were large numbers of loops lying on prism planes but this was not general, (Figure 7).

(b) Sample 287 - 22 (irradiated at 580 °C) showed the normal behaviour in prism flakes but flakes of basal orientation showed some very abnormal effects. Many large circular regions, 500 to 5000 Å in diameter were seen which contained two or more elliptical diffraction contours (Figure 8). The number of contours in a region depended on the number of strong diffracted beams, and their size was very sensitive to tilt.

The most probable explanation compatible with the observed diffraction effects is that these regions were voids, lenticular in cross-section, in the basal planes, (Izui and Fujita 1961) and the diffraction contours arose from distorted lattice planes adjacent to the voids.

Since the voids were never observed in prism flakes they must be formed when the basal flakes cleave away from the bulk material.

A possible explanation for their origin and also for the high proportion of basal flakes is that impurities lying in the basal planes reduce the cohesion in these planes. Then, under the tensile stress produced during fracture, the basal planes tend to separate at many different points, until in a particular plane the voids link together and fracture occurs.

(c) Sample 130 – 31 (irradiated at 1070 °C) showed relatively few dislocation loops. Extended stacking faults similar to those occasionally observed in unirradiated material were seen. Diffraction patterns from these areas showed characteristic streaking in the c direction. In addition, dislocation tangles were very common in this specimen.

Helium bubble formation was observed both in flakes and in replicas in some specimens. Bubbles were observed both within the grains and at the grain boundaries,(Figure 9), the former being the smaller and often having a crystallographic shape (Figure 10). No helium bubbles could be observed in the sample irradiated at 470 °C. In the range 580 – 895 °C some helium bubbles could occasionally be observed on grain boundary surfaces but bubble formation was not general and the observed bubbles accounted for an insignificant proportion of the total helium present. In sample 202 – 11 irradiated at 895 °C helium bubble formation was fairly general both within the grains and at the grain boundaries (Figure 9a). The samples irradiated at 1000 – 1100 °C all showed extensive helium bubble formation and the bubbles were larger in size than in sample 202 – 11 (Figure 9b). In the samples irradiated at 1200 °C, however, the helium bubble concentration and size was considerably less than in the samples irradiated at 1000 °C, that is, the expected variation with temperature was reversed at 1200 °C as was also the case with loop formation and lattice parameter change. The helium bubble formation in all samples was far too irregular to enable any meaningful estimate to be made of the contribution of helium bubbles to the total volume change. For specimen 169 – 8 for instance, by attempting an estimate of the mean bubble distribution one obtains a value of 0.5 ± 0.4 per cent. for the volume change due to helium. It is not possible from these figures to say how much of the difference between the X–ray volume change and the macroscopic volume change was due to helium.

One further observation of interest was that the proportion of cleavage failure in the fracture surfaces increased with increasing temperature up to 1000 °C but the samples irradiated at 1200 °C were again anomalous showing less cleavage failure than those irradiated at 1000 °C. This is presumably a result of decreasing anisotropic growth strain with increasing temperature. It also provides further confirmation that helium bubble formation itself does not significantly weaken the grain boundaries.

No apparent difference could be observed between samples containing ½ wt. per cent. MgO and the AOX samples when irradiation conditions were similar.

3.4 Effect of Irradiation at 1200 °C

The samples irradiated at 1200 °C showed anomalous behaviour in lattice parameter changes, defect cluster formation, amount of cleavage failure, and helium bubble formation. All the observations on these properties were more compatible with irradiation at around 700 – 800 °C rather than at 1200 °C. It is conceivable that this is a real effect and that above 1000 °C the cluster sizes start to decrease with a corresponding larger $\underset{\sim}{c}$ parameter change and that the helium gas is sufficiently mobile at these temperatures for a large proportion of it to escape from the sample and hence minimise bubble formation. Alternatively the observations could be due to the fact that these samples were irradiated during a reactor cycle in which there was a large amount of low power operation. Collins (private communication) has estimated that up to 25 per cent. of the total dose could have been accumulated at low power and hence at low temperatures. From our experience, damage produced at 500 – 700 °C would not anneal significantly at 1200 °C and the final damage in the material may then have been due to this damage produced at low temperatures rather than at 1200 °C. Insufficient information is available to distinguish between these two possibilities.

4. CONCLUSIONS

1. The lattice parameter changes, X–ray line broadening, and defect cluster formation in the General Electric samples were generally similar to those observed, or expected by extrapolation, in Lucas Heights samples. However it is difficult to draw firm conclusions because there were several anomalous samples, notably those irradiated at 1200 °C and one irradiated at 470 °C.

2. The results suggest that at 1000 – 1100 °C there is a significant anisotropic growth which is not reflected in the lattice parameters. The helium bubble formation at these temperatures was too irregular to allow an assessment of the contribution of this growth to the total volume change.

3. Variation of the dose rate by a factor of 5 to 10 does not have a major effect on the amount and nature of the damage. Small effects may be obscured by the inaccuracies in dose and temperature measurement.

4. Helium bubble formation in significant amounts only occurs at temperatures of 900 °C and above. Bubble formation occurs both within the grain and at grain boundaries.

5. No effects were observed which could be attributed to the 0.5 wt. per cent. MgO addition.

5. ACKNOWLEDGMENTS

Grateful acknowledgment is due to Mr. C. G. Collins of General Electric Company for arranging the supply of the samples and for many useful discussions on the work, and to the U.S.A.E.C. for permission to use the samples. The optical microscopy was carried out by P. Davis; K. G. Watson assisted with the X–ray studies and R. Blake with the electron microscopy.

6. REFERENCES

Chute, J. and Walker, D.G. (1964). – Proc. of Int. Conf. on BeO. (In press) North–Holland.

General Electric Company (1963). – Annual Progress Report N.M.P.O. Labs. G.E.M.P. 177A.

Hickman, B.S., Sabine, T.M., and Coyle, R.A. (1962). – J. Nucl. Mat. 6: 190.

Izui, K., and Fujita, F. (1961). – J. Phys. Soc. Japan 16; 1032.

Walker, D.G. (1963). – AAEC/TM 189.

Walker, D.G., Mayer, R.M., and Hickman, B.S. (1964). – Proc. of Int. Conf. on BeO. (In press) North–Holland.

TABLE 1

DETAILS OF SAMPLES SUPPLIED BY GENERAL ELECTRIC CO.

Composition	Specimen Number	Nominal		Test Number	Test Temp. °C	Dosage 10^{20} nvt ($\geq$ 1 MeV)	Flux 10^{14} nv ($\geq$ 1 MeV)	Irradiation Time 10^{6} seconds	Observed Volume Increase %
		Grain Size microns	Density g/cm^3						
	305–27	5	2.75	59	1200	4.14	3.11	1.33	0.36
UOX+0.5 w/o MgO	227–30	10	2.75	59	1200	4.22	3.20	1.33	0.36
	226–31	10	2.90	82	470	3.75	3.20	1.17	0.47
	202–8	10	2.90	50	750	8.70	1.93	4.50	1.38
	202–11	10	2.90	50	895	11.10	2.47	4.50	1.16
	202–30	10	2.90	59	1200	4.01	3.05	1.33	0.50
	117–6	20	2.90	58	840	2.96	2.45	1.21	0.35
	117–16	20	2.90	58	1011	3.32	2.74	1.21	0.41
	169–8	50	2.90	71	1080	5.05	2.14	2.36	0.71
AOX	315–20	10	2.75	59	1200	4.21	3.19	1.33	0.51
	120–27	20	2.90	58	766	2.61	2.16	1.21	0.85
	153–23	20	2.90	71	1000	5.32	2.25	2.36	0.72
	130–5	50	2.90	71	1005	5.90	2.50	2.36	0.71
	130–31	50	2.90	71	1070	3.45	1.46	2.36	0.61
	287–22	80	2.75	82	580	3.43	2.93	1.17	1.41

TABLE 2

RESULTS OF X-RAY DIFFRACTION STUDIES

Sample No.	Irrad. Temp. °C	c Parameter	a Parameter	$\frac{\Delta c}{c}$ %	$\frac{\Delta a}{a}$ %	$\frac{\Delta V}{V}$ (Theor)	$\frac{\Delta V}{V}$ (Macro)	Sharp Reflections Used for Determining c Parameter	Integral Breadth of 300 Cu Kα Reflection Deg. of θ
226 – 31 3.75×10^{20}	470	4.3921 ± 0.0006	2.6995 ± 0.0001	0.33	0.066	0.45	0.47	112, 103 CrK 302, 212, 105, 211 CuK	0.54
202 – 8 8.7×10^{20}	750	4.425 ± 0.010	2.6984 ± 0.0001	1.05	0.02	1.1	1.38	211 NiK 211 CuK	0.76
117 – 6 2.96×10^{20}	840	4.3852 ± 0.0005	2.6984 ± 0.0001	0.18	0.02	0.22	0.35	112, 103, CrK 211, 212, 302 CuK	0.37
202 – 11 11.1×10^{20}	895	4.43 ± 0.01	2.6981 ± 0.0001	1.2	–	1.2	1.34	211 NiK 211 CuK	0.39
117 – 16 3.32×10^{20}	1011	4.3797 ± 0.0008	2.6979 ± 0.0001	0.06	–	0.06	0.41	112 CrK 212, 211, 302 CuK	0.16
169 – 8 5.05×10^{20}	1080	4.3788 ± 0.0006	2.6976 ± 0.0001	0.03	–	0.03	0.71	112 CrK 212, 302, 211 CuK	0.26
227 – 30 4.22×10^{20}	1200	4.393 ± 0.0006	2.6979 ± 0.0001	0.3	–	0.3	0.36	211 NiK 211, 302 CuK	0.34
202 – 30 4.01×10^{20}	1200	4.3825 ± 0.0008	2.6978 ± 0.0001	0.11	–	0.11	0.50	112 CrK 211 CuK	0.38
287 – 22 3.43×10^{20}	580	4.3953 ± 0.0004	2.6979 ± 0.0001	0.41	–	0.41	1.41	112, 103 CrK 213, 302, 212, 105, 211 CuK	0.22
120 – 27 2.61×10^{20}	766	4.3897 ± 0.0003	2.6978 ± 0.0001	0.28	–	0.28	0.85	112, 103, CrK 211, 212, 302 CuK	0.26
153 – 23 5.32×10^{20}	1000	4.3796 ± 0.0006	2.6980 ± 0.0001	0.05	–	0.05	0.72	112 CrK 203, 212, 302, 211 CuK	0.48
130 – 5 5.9×10^{20}	1005	4.3832 ± 0.0008	2.6976 ± 0.0001	0.13	–	0.13	0.71	112 CrK 302, 114, 213, 211 CuK	–
130 – 31 3.45×10^{20}	1070	4.3772 ± 0.0002	2.6977 ± 0.0001	–	–	–	0.61	112, 103 CrK 105, 212, 302, 213, 114 CuK	0.35
315 – 20 4.21×10^{20}	1200	4.3848 ± 0.0006	2.6979 ± 0.0001	0.17	–	0.17	0.51	112 CrK 302, 211 CuK	–

TABLE 3

SUMMARY OF ELECTRON MICROSCOPY OBSERVATIONS ON HIGH TEMPERATURE IRRADIATED BeO

Specimen	Irradiation Temperature and Dose	Dislocation Loops	Helium Bubbles	Other Defects Observed	% Cleavage Fracture	Helium Bubbles on Intergranular Surfaces	Remarks
226 – 31	470 °C 3.75 x 10^{20} nvt	50–150 Å diameter. Smaller loops not resolved	None	Occasional stacking fault	20 – 30	None	Numerous fabrication pores 1 – 2μ diameter
202 – 8	750 °C 8.7 x 10^{20} nvt	150–400 Å diameter. Most loop planes $\perp$ to $\underset{\sim}{c}$ axis. Loops seen in both prism and basal flakes	Infrequent. 25–30 Å diameter	–	~ 10	$\leq$ 0.1μ. Numerous on some grain surfaces	Many fabrication pores 1 – 2μ on intergranular surfaces
117 – 6	840 °C 2.96 x 10^{20} nvt	Many loops 80–300 Å diameter. Some $\parallel$ to prism planes	None	A few long straight dislocation lines, $\perp$ to $\underset{\sim}{c}$ axis	40 – 50	None	Fabrication pores 1 – 3μ. Many with well developed terraces
202 – 11	895 °C 11.1 x 10^{20} nvt	Many loops, 400 – 1000 Å. Most lie in basal planes. Occasional flakes have many loops in prism planes	Many bubbles 30–50 Å diameter. Uniform distribution. Bubbles seen in prism flakes appear elongated along $\underset{\sim}{c}$ axis	Thin bands of stacking fault $\perp$ to $\underset{\sim}{c}$ axis. Many short lines ~ 100 Å, $\perp$ to $\underset{\sim}{c}$. Some long straight dislocations also $\perp$ to $\underset{\sim}{c}$	~ 50	0.1 to 0.3μ. Plentiful on most grain surfaces. Bubbles occasionally linked to form long narrow voids	Fabrication pores < 1μ on cleavage and intergranular surfaces. Up to 4μ at grain corners
169 – 8	1080 °C 5.0 x 10^{20} nvt	1–2 x 10^{15} loops/cm^3. 500–2000 Å diameter. Nearly all lie in basal planes	50–100 Å diameter in most flakes. 4–10 x 10^{15}/cm^3. In some basal flakes hexagonal bubbles up to 300 Å were seen	–	70 – 80	0.1 to 0.6μ. Concentration ranges from 0 to 5 x 10^8/cm^2 of grain surface. Many bubbles have crystallographic shapes	Fabrication pores 1 – 4μ on grain boundaries. < 1μ in grains
227 – 30	1200 °C 4.2 x 10^{20} nvt	250–600 Å diameter. Plentiful in all flakes. Most in basal planes	Very few. < 50 Å	–	~ 50	0.1 to 0.3μ on some grain surfaces. Most have crystallographic shape	Fabrication pores $\leq$ 2μ
202 – 30	1200 °C 4.01x 10^{20} nvt	Most in basal planes. 200–600 Å diameter. One flake contained many prism loops	Rare	A few dislocation tangles and some stacking faults	~ 20	0.1 to 0.6μ. High bubble density on some grain surfaces. None on others	Fabrication pores 1 – 2μ
287 – 22	580 °C 3.43 x 10^{20} nvt	50–150 Å diameter. High loop density. Most on basal planes	None	All basal flakes contain large lenticular voids. Viewed along $\underset{\sim}{c}$ axis they are 500–5000 Å diameter	~ 50	$\leq$ 0.1μ on some grain boundaries	Fabrication pores seldom < 2μ, occasionally > 12μ
153 – 23	1000 °C 5.32 x 10^{20} nvt	~ 2 x 10^{15} loops/cm^3. Basal loops 500–1200 Å diameter. A few prism plane loops, usually < 300 Å	~ 8 x 10^{15} bubbles/cm^3. 50–70 Å diameter. In prism flakes bubbles are elongated up to 150 Å in $\underset{\sim}{c}$ direction	A few stacking faults, $\perp$ to $\underset{\sim}{c}$	~ 60	0.1 – 1.0μ on most grain surfaces, crystallographic shapes	Fabrication pores 2 – 4μ
130 – 31	1070 °C 3.45 x 10^{20} nvt	500–1500 Å usually in basal planes. Loops are rare compared with 169–8 and 153–23	Some bubbles 30–50 Å occasional groups of larger bubbles. 100–200 Å	Many bands of stacking fault $\perp$ to $\underset{\sim}{c}$ axis. Dislocation tangles and helical dislocations prominent. Pronounced streaking of h O ℓ diffraction maxima in c* direction	~ 80	0.1 – 0.4μ on some boundaries. Less bubbles than in 169–8 and 153–23	Fabrication pores up to 20μ on some grain boundaries. 1–3μ within grains
315 – 20	1200 °C 4.21 x 10^{20} nvt	250–600 Å diameter ~ 4 x 10^{16}/cm^3. Mostly basal loops	Some bubbles. < 50 Å	Occasional dislocation lines and tangles. Some stacking faults and defect clusters	50 – 60	0.1–0.3μ on some boundaries	Fabrication pores 1 – 2μ. Maximum size 4μ. Occasionally linked on grain surfaces

TABLE 4

SUMMARY OF OPTICAL MICROSCOPY OBSERVATIONS

Sample No.	Irradiation Temperature °C	Dose > 1 MeV	Grain Size			Extent of Microcracking	Other Observations
			Nominal μ	Measured Longt. μ	Measured Transverse μ		
226–31	470	3.75×10^{20}	10	6	5	None observed	–
202–8	750	8.7×10^{20}	10	9	8.5	Extensive	Generally intergranular cracking
202–11	895	11.1×10^{20}	10	7.5	7	Limited	–
153–23	1000	5.3×10^{20}	20	15	15	Limited	Many grain boundaries showed strings of helium bubbles often linked by cracks
130–5	1005	5.9×10^{20}	50	36	40	Extensive	
130–31	1070	3.4×10^{20}	50	Not determined due to twinning		Limited	Very extensive twinning observed. Transgranular as well as intergranular cracking observed

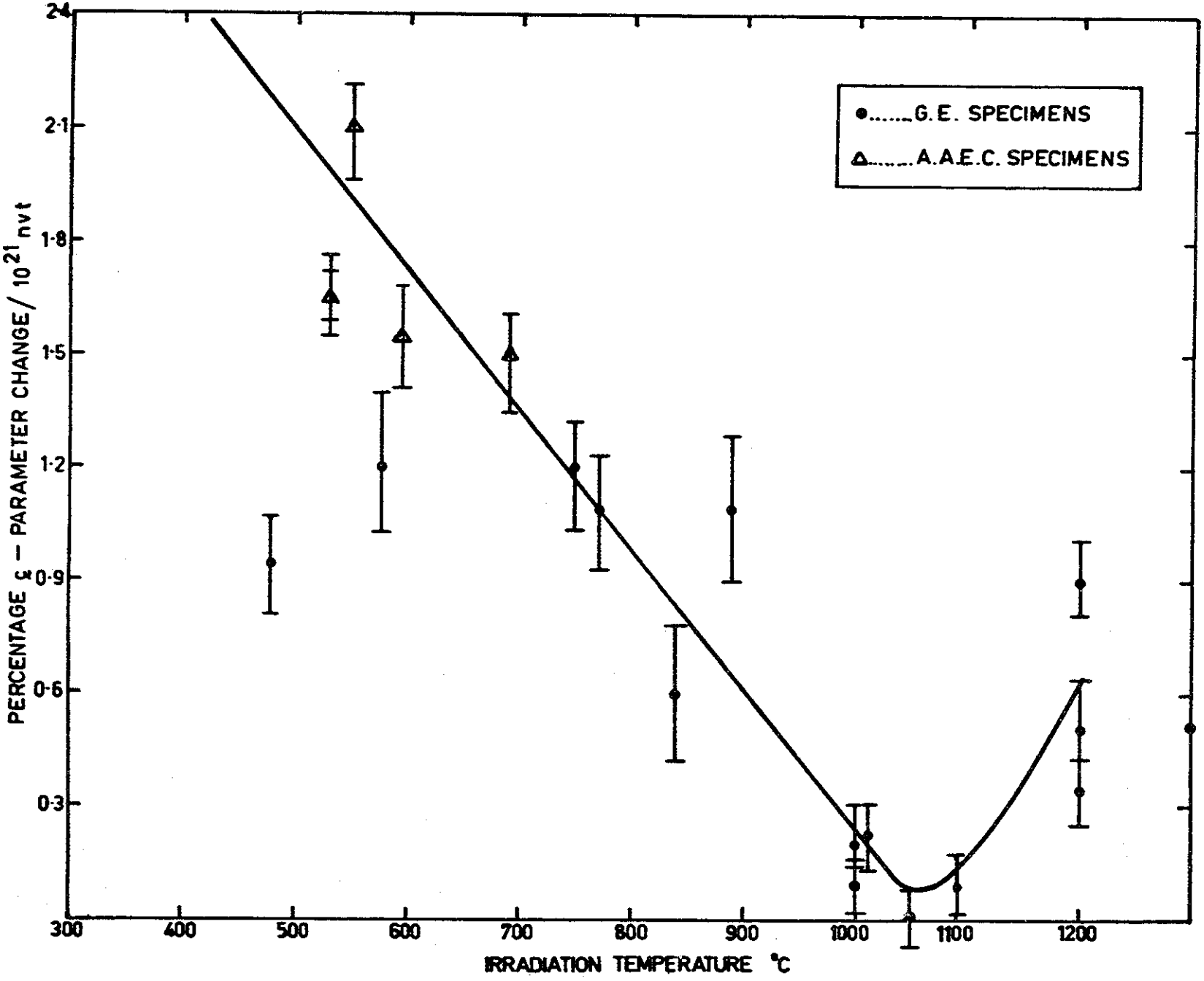

FIGURE 1 VARIATION IN c-PARAMETER CHANGE WITH IRRADIATION TEMPERATURE

P646

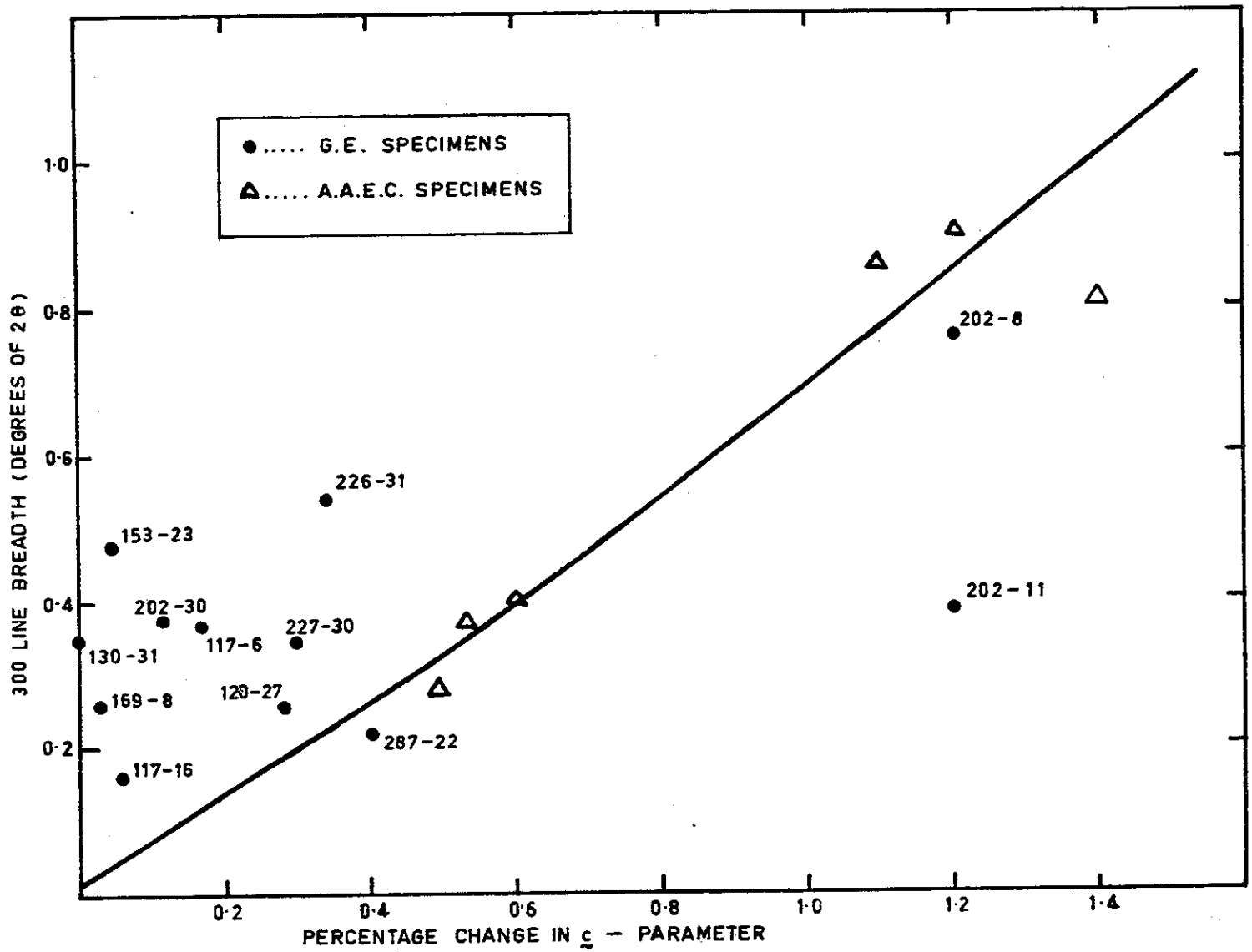

FIGURE 2. VARIATION OF BROADENING OF 300 Cu Kα REFLECTION WITH c-PARAMETER CHANGE

P646

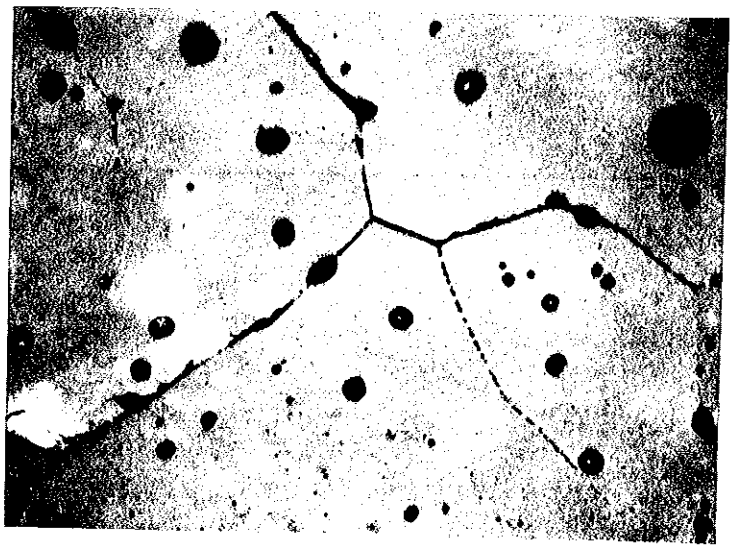

X 500

(a)

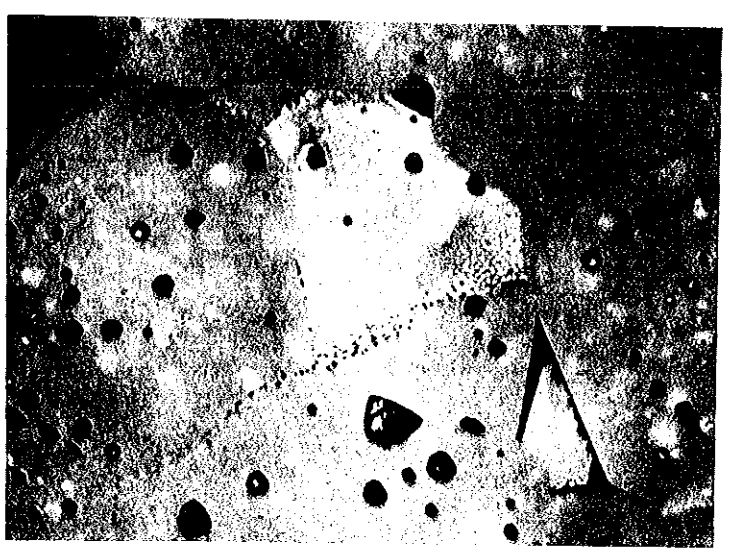

X 500

(b)

FIGURE 3. PHOTOMICROGRAPHS OF SAMPLE 130–5 SHOWING BUBBLE STRINGS AND ASSOCIATED MICRO–CRACKING. NOTE BUBBLE FORMATION ON SUB–SURFACE GRAIN BOUNDARY IN CENTRE OF FIGURE 3(b).

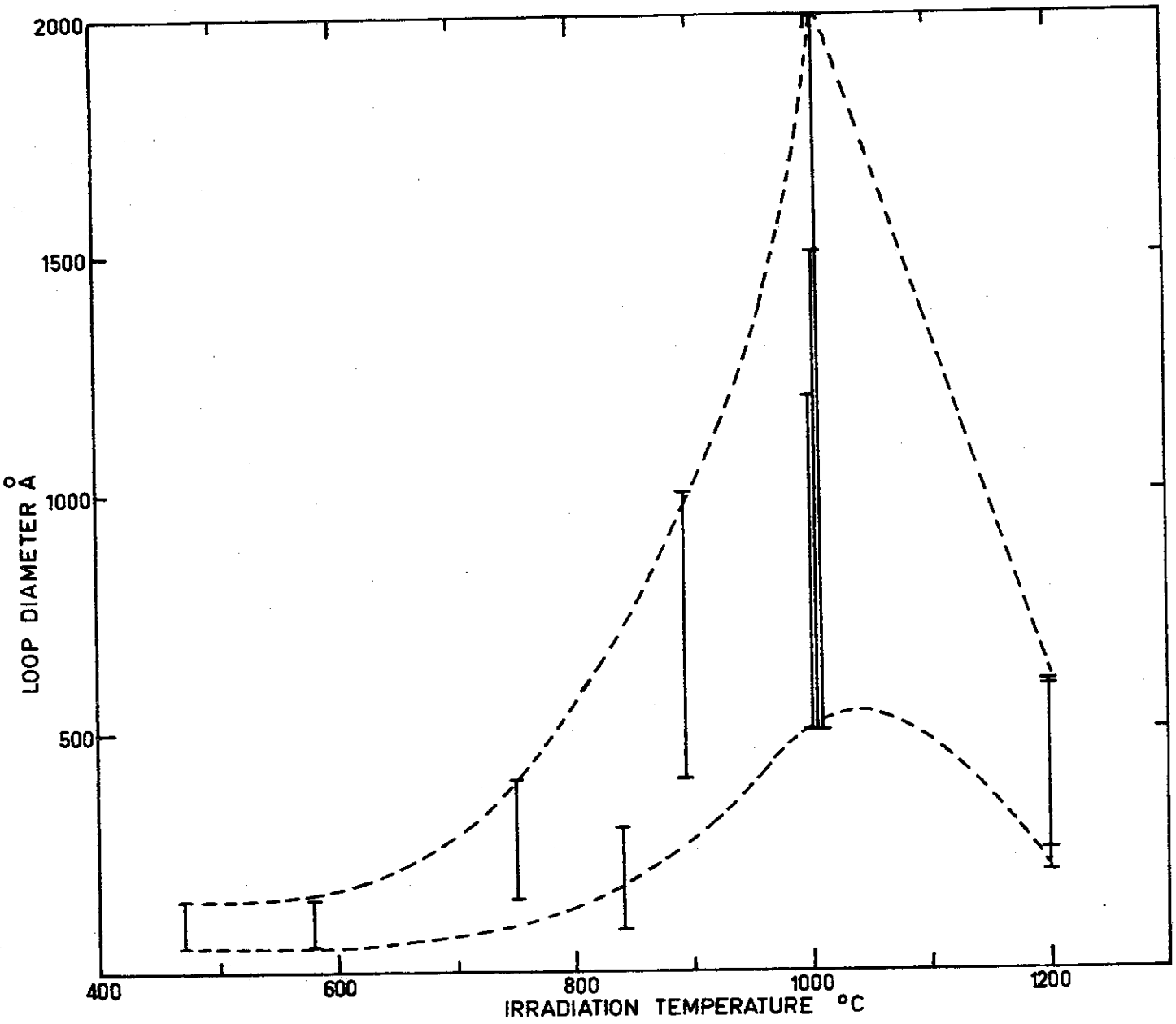

FIGURE 4. VARIATION OF LOOP DIAMETER WITH IRRADIATION TEMPERATURE

P646

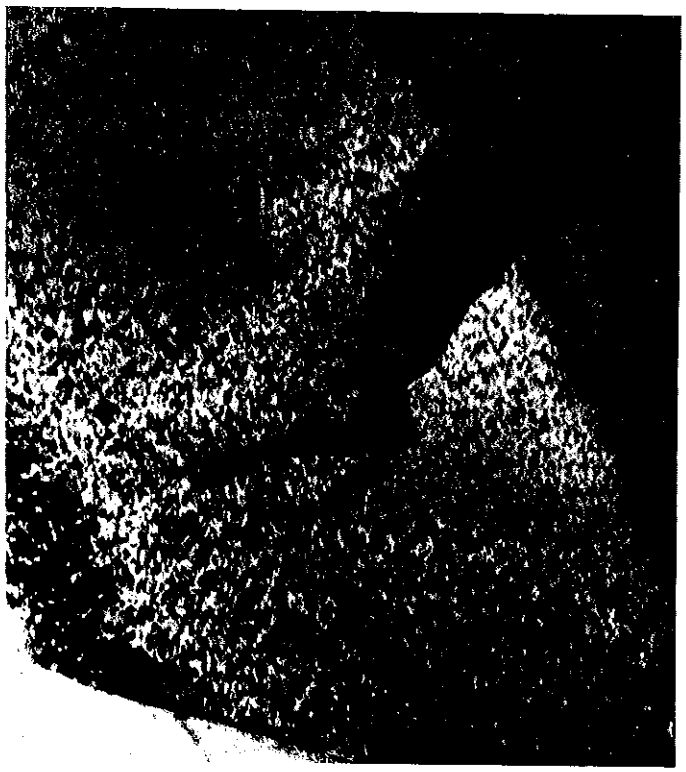

X 120,000

(a) Specimen 226–31 (470 °C)

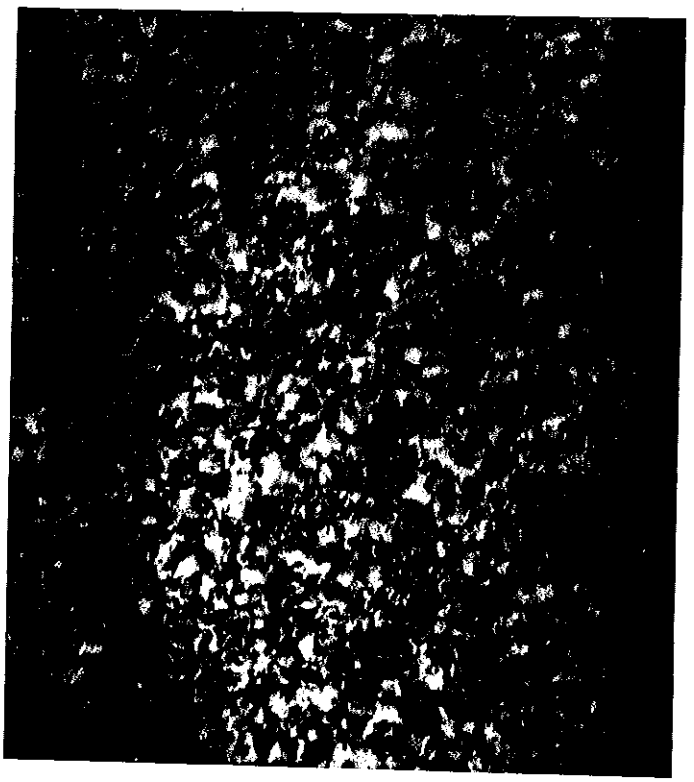

X 100,000

(b) Specimen 202–8 (750 °C)

X 120,000

(c) Specimen 202–11 (895 °C)

X 80,000

Basal Flake

X 90,000

Prism Flake

(d) Specimen 169–8 (1080 °C)

GURE 5. DEFECT CLUSTERS AND DISLOCATION LOOPS IN NEUTRON IRRADIATED BeO, SHOWING INCREASE IN SIZE WITH INCREASE IN IRRADIATION TEMPERATURE, UP TO 1000 °C

FIGURE 6.

TYPICAL DISLOCATION LOOPS LYING IN THE BASAL PLANES OF A BeO FLAKE (315–20) AFTER IRRADIATION AT 1200°C

X 100,000

FIGURE 7.

DISLOCATION LOOPS ON PRISM PLANES IN A BeO FLAKE (202–30) AFTER IRRADIATION AT 1200°C

X 60,000

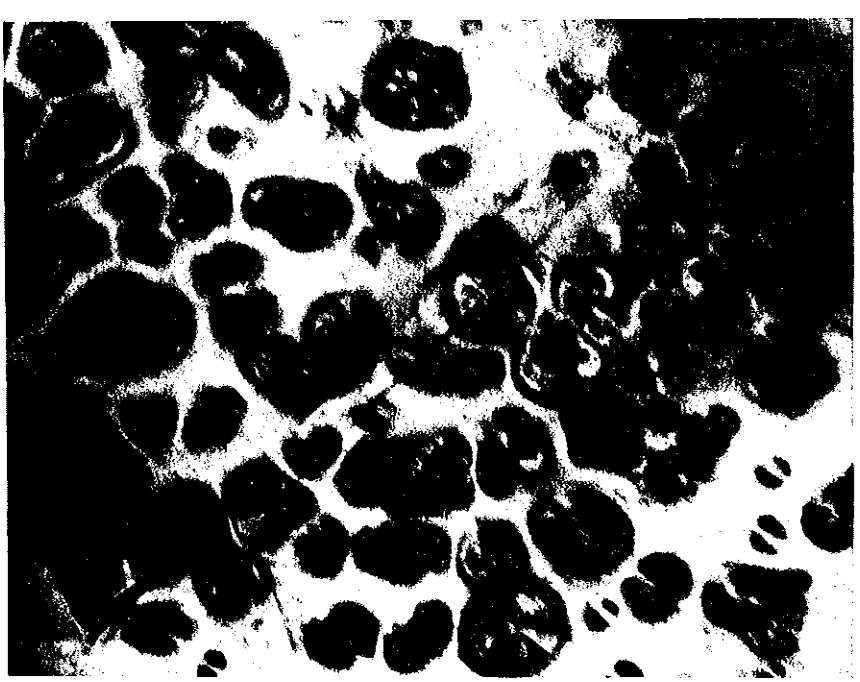

FIGURE 8.

LENTICULAR VOIDS IN A BASAL FLAKE FROM SPECIMEN 287–22

X 32,000

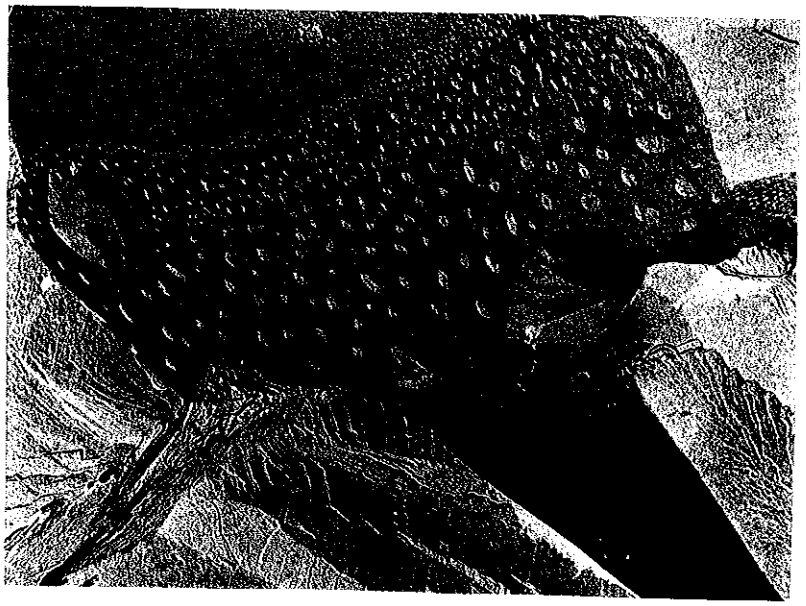

(a) Specimen 202–11

X 15,000

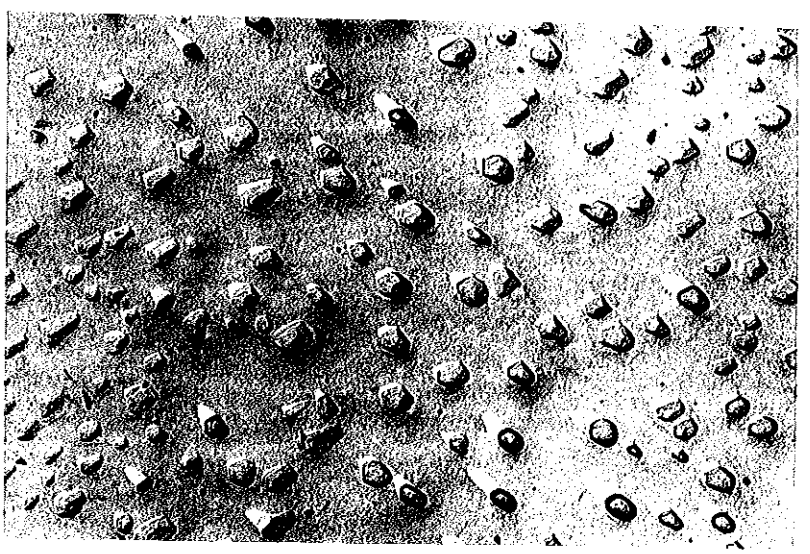

(b) Specimen 169–8

X 15,000

FIGURE 9. HELIUM BUBBLES ON INTERGRANULAR SURFACES IN BeO AFTER NEUTRON IRRADIATION AT (a) 895 °C AND (b) 1080 °C

X 120,000

FIGURE 10. HELIUM BUBBLES IN A BASAL FLAKE FROM SPECIMEN 130–31, AFTER NEUTRON IRRADIATION AT 1070 °C